Using simplistic shape/surface models to predict brightness in estimation filters

Charles J. Wetterer, Bobby Hunt, David G. Sheppard
Integrity Applications Incorporated - Pacific Defense Solutions

CONFERENCE PAPER

The prerequisite for using brightness (radiometric flux intensity) measurements in an estimation filter is to have a measurement function that accurately predicts a space object's brightness for variations in the parameters of interest. These parameters include changes in attitude and articulations of particular components (e.g. solar panel east-west offsets to direct sun-tracking). Typically, shape models and bidirectional reflectance distribution functions are combined to provide this forward light curve modeling capability. To achieve precise orbit predictions with the inclusion of shape/surface dependent forces such as radiation pressure, relatively complex and sophisticated modeling is required. Unfortunately, increasing the complexity of the models makes it difficult to estimate all those parameters simultaneously because changes in light curve features can now be explained by variations in a number of different properties. The classic example of this is the connection between the albedo and the area of a surface. If, however, the desire is to extract information about a single and specific parameter or feature from the light curve, a simple shape/surface model could be used. This paper details an example of this where a complex model is used to create simulated light curves, and then a simple model is used in an estimation filter to extract out a particular feature of interest. In order for this to be successful, however, the simple model must be first constructed using "training" data where the feature of interest is known or at least known to be constant.

1. INTRODUCTION

The utility of using brightness (radiometric flux intensity) measurements to determine a space object (SO)'s attitude and shape has been long established [1]. Ref. [2] first demonstrated how these brightness measurements can also be used in an estimation filter, such as the unscented Kalman filter (UKF) [3,4], to estimate the attitude and angular rates of a SO. Multi-bandpass observations, fusion with angles measurements, multiple hypothesis testing, and simultaneous estimation with position, velocity, attitude, angular rates, surface parameters and mass have also been demonstrated [5,6,7]. In all these implementations, however, an accurate shape/surface model was needed and used within the filter to provide a forward light curve modeling capability. Whereas modeling uncertainties introduce a systematic error in the UKF's resulting final state, these can be mitigated by incorporated the uncertainties as "consider" parameters using an unscented Schmidt Kalman filter (USKF) [8,9,10].

Sometimes, however, an adequate shape/surface model is not available and must be constructed from scratch. This paper aims to demonstrate this process while showing the successful implementation of a simplistic shape/surface models in an estimation filter.

2. DETAILS OF APPROACH

In this paper, the USKF is used to estimate the solar panel articulation angles of a three-axis stabilized geosynchronous Earth-orbit (GEO) satellite using light curves as input. Initially, however, the USKF is also used to construct a simple shape/surface model for the filter's measurement function. In all cases, a number of parameters associated with the shape/surface model are estimated and contained in a state vector. The state vector consists of those parameters being estimated and so-called "consider" parameters whose uncertainty is being considered but whose values remain fixed.

$$\hat{z}_{USKF} = \begin{bmatrix} x^1 & \dots & x^{n_x} & c^1 & \dots & c^{n_c} \end{bmatrix}^T \tag{1}$$

where x are the n_x estimated parameters, and c are the n_c considered parameters and $\hat{z}$ is the USKF's state. The state has an associated covariance.

$$P_{USKF} = P_{zz} = \begin{bmatrix} P_{xx} & P_{xc} \\ P_{cx} & P_{cc} \end{bmatrix} \tag{2}$$

The state parameters are propagated forward in time with a dynamics, or state, function.

$$\hat{z}_k^- = f\left(\hat{z}_{k-1}^+, w_k\right) \tag{3}$$

where w_k is the process noise vector and (3) shows the state going from the a posteriori state at time step k-1 to the a priori state at time step k. The general measurement function is

$$\hat{y}_k = h\left(\hat{z}_k^-, v_k\right) \tag{4}$$

where v_k is the measurement noise vector and y is a vector representing the m observations.

In this paper, multiple hypotheses with different initial states are processed simultaneously and weighted according to how well they predict the observations. Each hypothesis is a separate instantiation of the USKF. Generally, this architecture is that of the Unscented Particle Filter (UPF) first proposed by van der Merwe et al. [11]. As such, "particles" and "hypotheses" represent the same thing. The resampling step of the UPF is not utilized, and thus this UPF implementation is essentially identical to Multiple Model Adaptive Estimation (MMAE) [12,13]. The conditional probability for the i-th hypothesis and k-th time step is calculated using

$$p_k^i = (2\pi)^{-m/2}\left|P_{yy,k}^i\right|^{-\frac{1}{2}} e^{-\frac{1}{2}\left(\hat{y}_k^i - \tilde{y}_k\right)\left(P_{yy,k}^i\right)^{-1}\left(\hat{y}_k^i - \tilde{y}_k\right)} \tag{5}$$

where $\tilde{y}_k$ are the actual measurements and $P_{yy,k}^i$ is the calculated innovation covariance within the filter. The likelihood function that expresses the weight for the i-th hypothesis at the k-th time step is then

$$w_k^i = \frac{p_k^i}{\sum_{i=1}^{N} p_k^i} \tag{6}$$

where N is the total number of hypotheses. These weights are used to generate a composite solution at the end of the estimation.

3. DETAILS OF SCENARIO

The scenario used in this paper is that of a satellite at GEO whose attitude is such that its primary axis (z-axis) is pointing at a particular latitude and longitude on the surface of the Earth, and its secondary axis (x-axis) is pointing as close to the velocity vector of its orbit as possible. The model satellite has solar panels that project along the third direction (±y-axis). The solar panels track the Sun but also have an unknown E-W articulation angle from exact primary axis pointing. The full model satellite is shown in Fig. 1a while the simplified model satellite is shown in Fig. 1b.

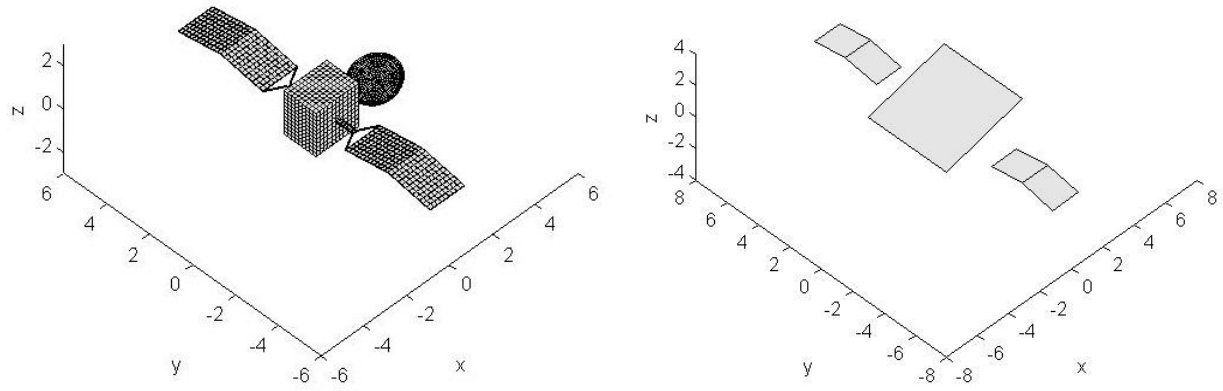

Figure 1 –Satellite models (a) full, and (b) simplified

In the full model, each surface is divided into many smaller facets to allow for self-shadowing or obscuration of portions of the surface. The small angle between the two halves of the solar panel along its length will be referred to as the "deployment angle" and is set here to 10 degrees. The solar panels in the simplified model are set to the same size as in the full model so a direct comparison between the estimated values and the truth values can be accomplished, although this need not be the case. Essentially, if the solar panels were made bigger, the

corresponding reflectance values would be correspondingly smaller. The "bus" facet in the simplified model, however, is deliberately set larger (shown at 5 meters across in this figure) to keep the reflectance values reasonable for it must account for the specular glint off the parabolic dish in the full model. The bus facet in the simplified model is also tilted in the E-W direction (shown at -15 degrees in this figure) to account for the asymmetry in the full model caused again by the parabolic dish. The full model has 3050 total facets while the simplified model has only 5 facets. The significantly smaller number of facets in the simplified model allows for a correspondingly larger number of hypotheses to be generated and tested while keeping the computational burden the same.

The satellite is placed in the orbit of Galaxy 15 (SSN28884) using the historic two-line elements (TLEs). There are two periods of observation. In the first period, referred to as the "training" set (2012 Jan 01 to 2012 Dec 31), the E-W articulation angles of the solar panels remain fixed (6^o and 1^o) and the satellite is observed one hundred times over the course of the year. In the second period, referred to as the "operations" set (2013 Jan 01 to 2013 Dec 31) the satellite is observed eighty times over the course of the year but for half the days the E-W articulation angles are slightly different from the "nominal" values of the prior year. The goal of the simulation is to identify these "anomalous" days using the estimation filter. The results using the full shape/surface model will be compared to the results using a simplistic shape/surface model constructed with the training set.

For the full model used to generate the truth, the rectangular bus and parabolic dish, and the solar panels and connectors are represented by different Bidirectional Reflectance Distribution Functions (BRDFs). The specific BRDF surface model is the Cook-Torrance BRDF [14] with the "truth" values listed in Table 1. Additionally, the deployment angle is set to 10^o and remains fixed throughout. Also listed in Table 1 are estimate values (randomly corrupted using the associated uncertainty) to be used with the full shape/surface model analysis of Section 5.

Table 1. Full model surface BRDF parameters

	Bus/Dish truth	Solar panels truth	Bus/Dish estimate	Solar panels estimate
microfacet slope (m)	0.10	0.05	0.0983 ± 0.0050	0.0567 ± 0.0050
B reflectance (ρ_B)	0.90	0.70	0.8742 ± 0.0500	0.6868 ± 0.0500
B diffuse fraction (d_B)	0.70	0.20	0.6864 ± 0.0500	0.2316 ± 0.0500
V reflectance (ρ_V)	0.85	0.65	0.8374 ± 0.0500	0.6524 ± 0.0500
V diffuse fraction (d_V)	0.68	0.17	0.7360 ± 0.0500	0.1839 ± 0.0500

The satellite is observed in two wavebands from the location of the Advanced Electro-Optic System (AEOS) on Maui, Hawaii for thirty-seven measurements starting at 06:00:00 UT with 600s time step (6 hours). The measurement vector is

$$\tilde{y} = \begin{bmatrix} B & V \end{bmatrix}^T \tag{7}$$

The measurement noise values are used corresponding to base uncertainty of 0.04 magnitudes and a random Poisson statistics error corresponding to a zero point of magnitude 20.8. Sample light curves using the full model are shown in Fig. 2. The first light curve is during a time when the specular glint off the solar panels is not observed. The second light curve is during a time when the solar panel glint is near maximum.

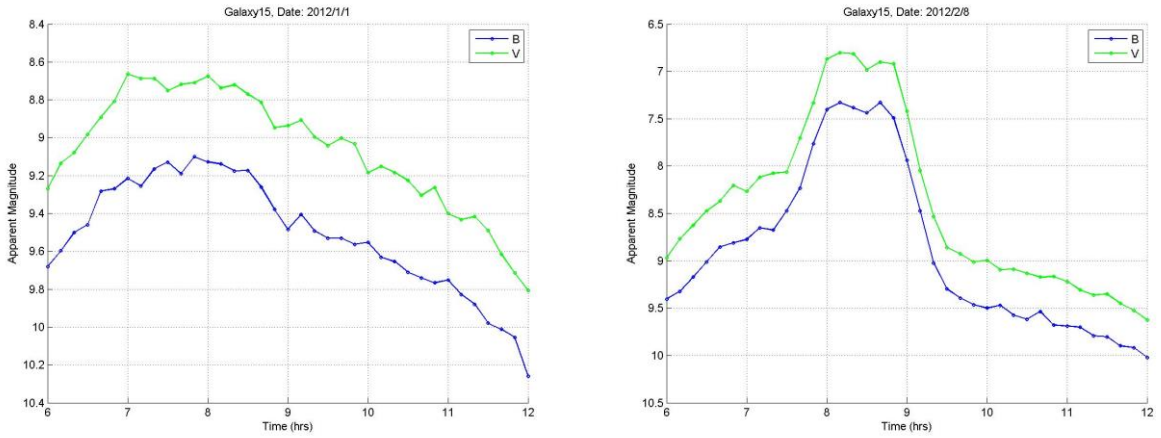

Figure 2 – B and V waveband truth light curves for "training" day on Jan 1 and Feb 8.

4. TRAINING THE SIMPLE MODEL

The parameters of the simple model will be determined iteratively in the spirit of coordinate descent optimization. Namely, after an initial manual adjustment, the parameters associated with the bus facet will first be estimated using a USKF estimation filter. These parameters will then be held fixed while the parameters associated with the solar panels are then estimated. This process will be repeated twice more to ensure the simplified model is adequately reproducing the "training" set of light curves from the first year and the values have converged. Any remaining differences will be reflected in the uncertainties assigned to the BRDF parameters in the simple model.

The first step is to create a simple model that is in the ballpark. This is achieved by using the two days depicted in Fig. 2 (Jan 1 and Feb 8). The Jan 1 light curve is dominated by the reflectance of the bus facet while Feb 8 has the maximum solar panel contribution. No prior knowledge is assumed, so a total of 14 parameters need to be roughly estimated. These are shown in Table 2 with the corresponding values and uncertainties estimated from this manual adjustment. Also shown in Table 2 are the results from subsequent steps to be described in the rest of this section and the truth values for the solar panel from Table 1. After step 1, bus parameters are changed in the even steps while solar panel parameters are changed in the odd steps.

Table 2. Simple Model Parameter Values

Parameter	step 1	step 2/ step 3	step 4/ step 5	step 6/ step 7	truth
Bus microfacet slope (m)	0.100 ± 0.005	0.1066 ± 0.005	Empirical(step4)	Empirical(step6)	
Bus B reflectance (ρ_B)	0.50 ± 0.05	0.6728 ± 0.05	Empirical(step4)	Empirical(step6)	
Bus B diffuse fraction (d_B)	0.70 ± 0.05	0.4449 ± 0.05	Empirical(step4)	Empirical(step6)	
Bus V reflectance (ρ_V)	0.475 ± 0.05	0.5804 ± 0.05	Empirical(step4)	Empirical(step6)	
Bus V diffuse fraction (d_V)	0.70 ± 0.05	0.4826 ± 0.05	Empirical(step4)	Empirical(step6)	
Bus E-W offset angle	-17	-18.1	Empirical(step4)	Empirical(step6)	
Panel microfacet slope (m)	0.060 ± 0.005	0.0548 ± 0.0060	0.0502 ± 0.0017	0.0499 ± 0.0012	0.05
Panel B reflectance (ρ_B)	0.50 ± 0.05	0.6483 ± 0.0385	0.6589 ± 0.0154	0.6616 ± 0.0083	0.70
Panel B diffuse fraction (d_B)	0.30 ± 0.05	0.1935 ± 0.0417	0.1833 ± 0.0137	0.1804 ± 0.0076	0.20
Panel V reflectance (ρ_V)	0.50 ± 0.05	0.6481 ± 0.0351	0.6540 ± 0.0134	0.6558 ± 0.0085	0.65
Panel V diffuse fraction (d_V)	0.30 ± 0.05	0.2069 ± 0.0399	0.2020 ± 0.0146	0.2008 ± 0.0088	0.17
Panel deployment angle	11	10.0	10.11	10.14	10
Panel articulation angle #1	5 ± 1	5.70 ± 0.42	5.95 ± 0.14	6.00 ± 0.11	6
Panel articulation angle #2	0 ± 1	1.03 ± 0.23	1.05 ± 0.10	1.06 ± 0.08	1

Step 2 uses the estimation filter to refine the bus facet values while keeping the solar panel facet values fixed. The Jan 1 light curve in Fig 2, which again is dominated by the contribution from the bus facet, is used. 560 different hypotheses are generated corresponding to 7 different values for the bus E-W offset angle (-20 to -14 degrees), 5 different microfacet slope values (step 1 value, $\pm 2\sigma$ from this value, and $\pm 4\sigma$ from this value), and 2 different reflectance and diffuse fraction values ($\pm\sigma$ from step 1 value). The final weights for all the hypotheses are used to determine the final values with the uncertainties reset to the original. These values are shown in Table 2. Note that these values are not necessarily close to the truth values as listed in Table 1 since the size of the facet was also adjusted in step 1 to keep reasonable values for the reflectances.

Step 3 uses the estimation filter to refine the solar panel facet values while keeping the bus facet values fixed, this time with the associated bus facet uncertainty considered. The light curves from six early training days (Jan 25, 29, Feb 2, 4, 8, 12) are used which all have strong solar panel glints. For each, 576 different hypotheses are generated corresponding to 4 different deployment angles (8 to 11 degrees), 3 different solar panel articulation angles (step 1 values, $+2\sigma$ from these values for both angles, -2σ from these values for both angles), 3 different microfacet slope values (step 1 value, $\pm\sigma$ from this value), and 2 different reflectance and diffuse fraction values ($\pm\sigma$ from step 1 value). For this step, good light curve fits are achieved for every deployment angle by adjusting the reflectance and diffuse fraction values. This is an example of parameters within the model that are linked and produce similar changes in the light curve. The best deployment angle, however, can be calculated by determining the angle at which the differences in reflectance and diffuse fraction between the days are minimum. This is shown in Fig. 3 which plots the BRDF parameters for the six days. Once the value of the best deployment angle is determined, the estimates for the other solar panel values can be calculated using the final estimates for those hypotheses with that deployment angle. The uncertainties are calculated as the average final uncertainty values from the estimation filter combined in quadrature with the standard deviation of the values from each day. Again, these are shown in Table 2.

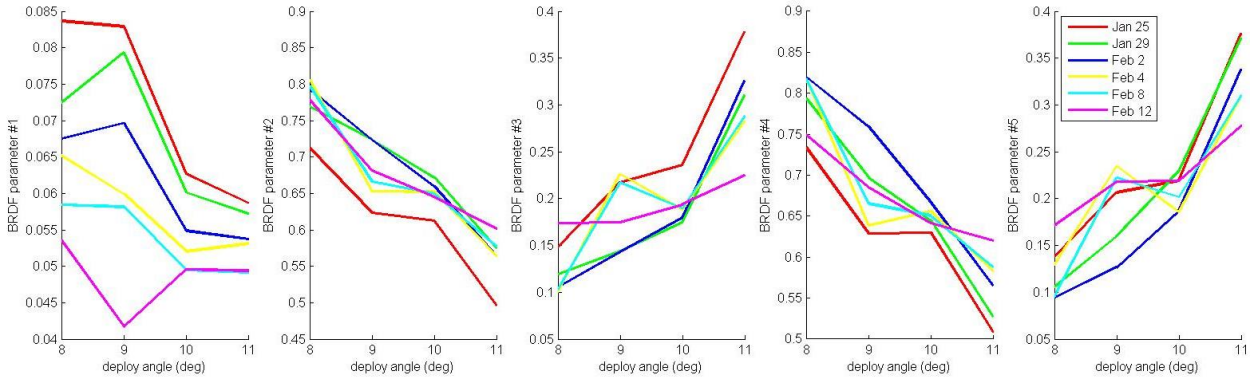

Figure 3 – BRDF values as function of deployment angle from step 3 analysis of training set.

A single set of values for the bus facet is insufficient to duplicate the brightness reflected by the full model's bus and parabolic dish throughout the year with changing orientation with respect to the Sun and observer. Thus, step 4 returns to estimating the bus values, now using the entire training set (100 days), while keeping the solar panel values from step 3 constant and considering their uncertainty within the filter. 36 different hypotheses corresponding to 12 E-W offset angles (-26 to -15 degrees) and 3 different microfacet slope values (step 2 values, $\pm 2\sigma$ from this value). For each day, the previous day's final result is used to generate the hypotheses. The results can be used to construct an empirical function to extract the bus BRDF parameters and uncertainties and the bus E-W offset angle as a function of day of year.

Step 5 now repeats the step 3 analysis using the step 4 results for the bus values instead of the step 2 results. In this case, all training days throughout the year with strong solar panel glints are used for twenty-six in total (Jan 25, 29, Feb 2, 4, 8, 12, 14, 20, 24, 26, Jun 7, 13, 15, 21, 23, 27, Jul 3, Oct 15, 17, 21, 23, 27, 31, Nov 2, 10, 12). For each, 11 different hypotheses are generated corresponding to 11 different deployment angles (step 3 value, ± 0.5 degrees from this value in 0.1 degree increments). An identical analysis as done in step 3 is accomplished to determine the best deployment angle and the corresponding BRDF parameters and solar panel articulation angles.

Step 6 then repeats the step 4 analysis using the step 5 results for the solar panel values instead of the step 3 results. 12 different hypotheses corresponding to the same 12 E-W offset angles and the same training days are used with the results again being an empirical function for the bus BRDF parameters and uncertainties and the bus E-W offset angle as a function of day of year. Figures 4 and 5 display the evolution of these bus value empirical functions from step 1 (black), step 2 (gray), step 4 (red), and step 6 (blue). The latter two steps produce and represent repeatable and seasonally dependent empirical functions. There is not much difference in these two steps indicating convergence to a "best" solution for the bus parameters has been reached and step 6 was probably unnecessary.

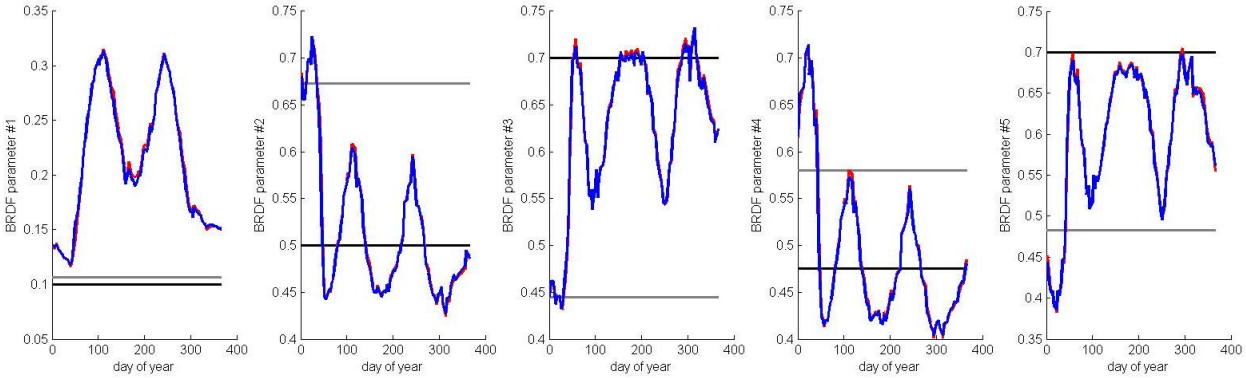

Figure 4 – Empirical functions for Bus BRDF parameters for various steps in process.

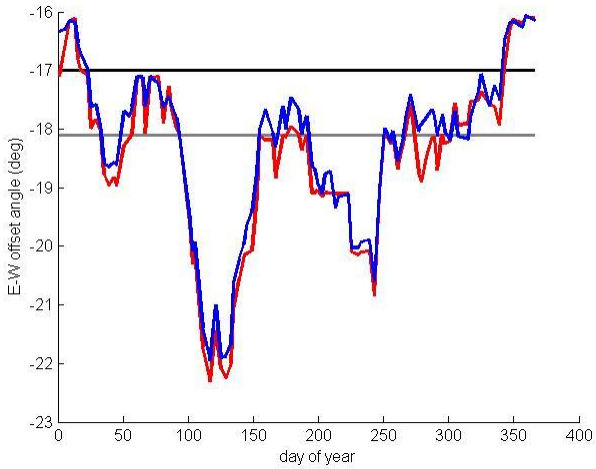

Figure 5 – Empirical functions for Bus E-W offset angle for various steps in process.

Finally, step 7 now repeats the step 5 analysis using the step 6 results for the bus values instead of the step 4 results. The same days and hypotheses are used and an identical analysis as done in step 5 is accomplished to determine the best deployment angle and the corresponding BRDF parameters and solar panel articulation angles. Figures 6 and 7 display the evolution of the estimated solar panel values from step 1 (black), step 3 (gray), step 5 (red) and step 7 (blue) as compared to the truth (green). The values do converge nicely close to the truth in all cases, although some parameters have a residual systematic error. Again there is not much difference in values in the last two steps indicating convergence to a "best" solution for the solar panel parameters and step 7 was probably unnecessary.

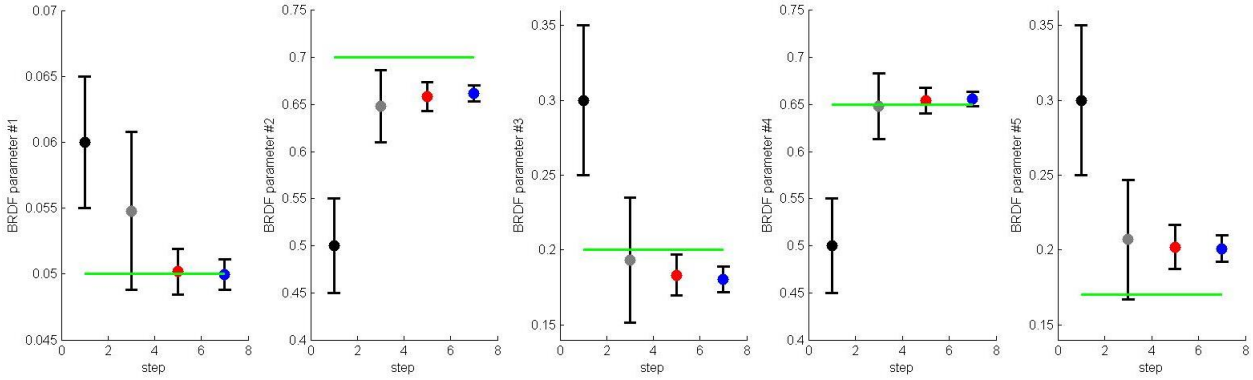

Figure 6 – Solar Panel BRDF parameters for various steps in process. Truth values shown as horizontal green lines.

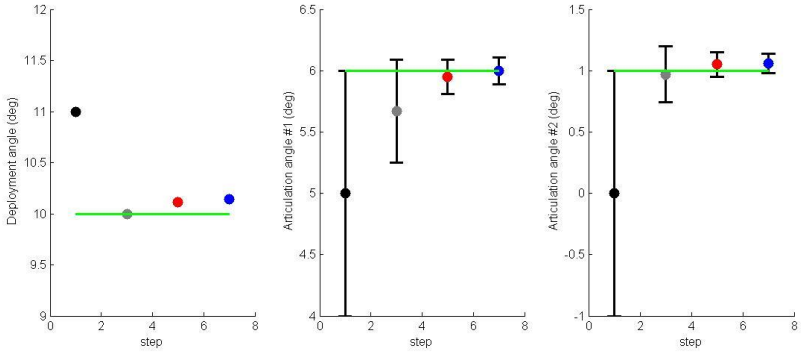

Figure 7 – Solar Panel deployment angle, and articulation angles for various steps in process. Truth values shown as horizontal green lines.

In this demonstration, the values from one year (training set) are used to predict the values to use in the next year (operations set). Alternatively, with a high volume of observations, the previous few days could be used to project what parameters to use for the current day's observations.

5. RESULTS

The operations set can now be analyzed using the simple model constructed in the previous section. For each day, the USKF will estimate the solar panel articulation angles while considering the uncertainties in the BRDF parameters. Twelve different hypotheses with solar panel articulation angle combinations distributed in a 2 degree grid between -2 and 9 degrees ($\theta_1 > \theta_2$) are used with initial uncertainties of 1 degree and centered on the nominal values.

The probability distribution function (pdf) built from a weighted Gaussian mixture of the final states for the different hypotheses is constructed, and the pdf value associated with the "nominal" articulations found from the training set is then calculated. It is the associated "sigma" value (constrained to be between 0.1 and 10) as determined by the probabilities (i.e. 1σ contour corresponds to the fraction 0.6827 of the pdf contained within) that is used to determine whether a particular day is considered "nominal" or "anomalous".

Figure 8 shows example results for a particular day (Jan 16) in the operations set. The initial hypothesis states are shown in black, the final estimated states are shown in red, the composite state accounting for the final weights is shown in green, the "nominal" state (as determined from the training set) is shown in blue, and the 1σ, 2σ, and 3σ pdf contours are shown as green lines. For this particular day (anomalous ($\theta_1 = 7^o$, $\theta_2 = 1.5^o$) solar panel articulation angles), the resulting "sigma" value is 2.80.

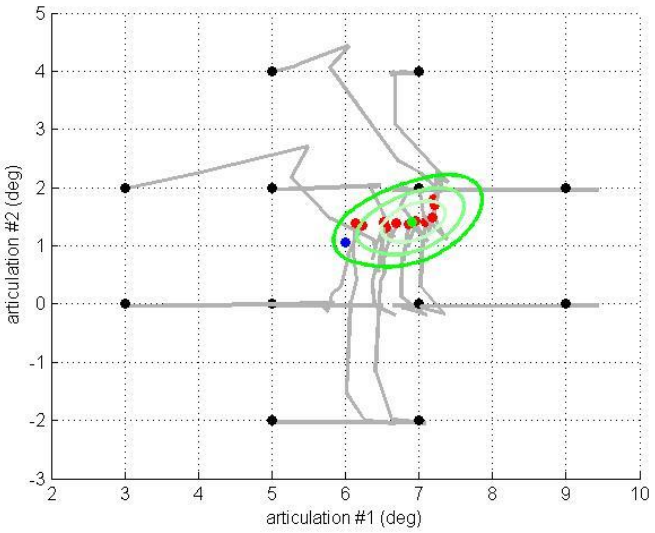

Figure 8 – USKF results for operations day Jan 16 (simple model)

Figure 9 displays these pdf sigma values (as calculated using results similar to those shown in Figure 8) for all of the 80 days in the operations set for both the case where the full shape/surface model is used and the case where the simple model is used. For the full shape/surface model, the truth values for deployment angle and nominal solar panel articulation angles are assumed known. A small uncertainty in the BRDF parameters in the model is implemented (see Table 1) and this uncertainty is considered within the USKF. For the simple model, the values as determined with the training set and described in the previous section are used. In the figure, Green dots correspond to days where the truth is "nominal" ($\theta_1 = 6^o$, $\theta_2 = 1^o$), while yellow dots ($\theta_1 = 5.5^o$, $\theta_2 = 1.5^o$) and red dots ($\theta_1 = 7^o$, $\theta_2 = 1.5^o$) correspond to "anomalous" days.

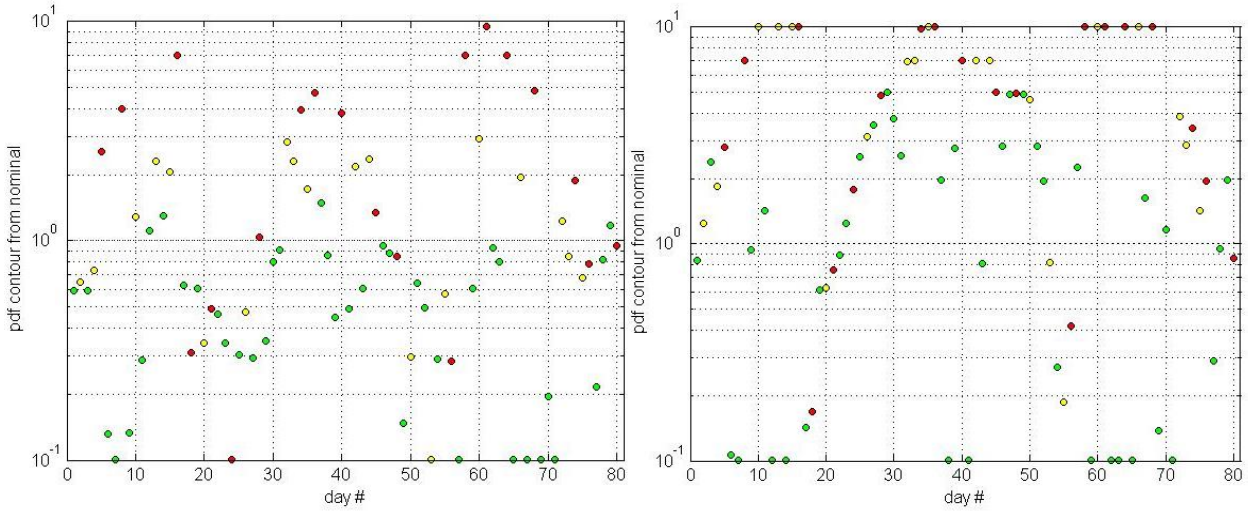

Figure 9 – PDF sigma values of operations set for (a) full shape/surface model with BRDF uncertainties and (b) simple model

The larger average value for the pdf contour for nominal days indicates the simplistic model has residual shape uncertainties not accounted for by the BRDF uncertainties considered in the estimation filter. The BRDF uncertainties could be inflated to account for this, but the separation between nominal and anomalous days would likely be unaffected. The overall performance for the two cases can be judged by constructing a Receiver Operations Characteristic (ROC) curve. This is achieved by varying the sigma value threshold of the boundary between nominal and anomalous days and comparing to the known truth. The resulting ROC curves for both the

full shape/surface model with BRDF uncertainties and simple model are shown in Fig. 10. To compare the performance quantitatively, the "area under the curve" (AUC) for the ROC curves are calculated. There is actually a slight improvement in performance with the resulting AUC values equal to 0.80 and 0.82 respectively, although this is within the approximate 0.05 uncertainty in this value. This uncertainty was estimated using randomly generated distributions (Gaussian, uniform, and heavy tail Lambert W of Gaussian) of various widths and separations and the average and standard deviations of the resulting AUC values for the ROC curves given a sample size of N = 80. When the full model is used with no BRDF errors and small uncertainty ($\sigma_m = 0.001$, $\sigma_\rho = \sigma_d = 0.01$), the resulting AUC value is 0.88 ± 0.04. This represents optimal filter performance, for there are some periods during the year when the specular glint off the solar panel is not observable and thus the solar panel articulation angles simply can't be estimated. Although it is now evident that the simplistic model (and of course the full model with BRDF uncertainties) do not perform optimally, they still perform well for the AUC uncertainty ranges still overlap with the optimal case.

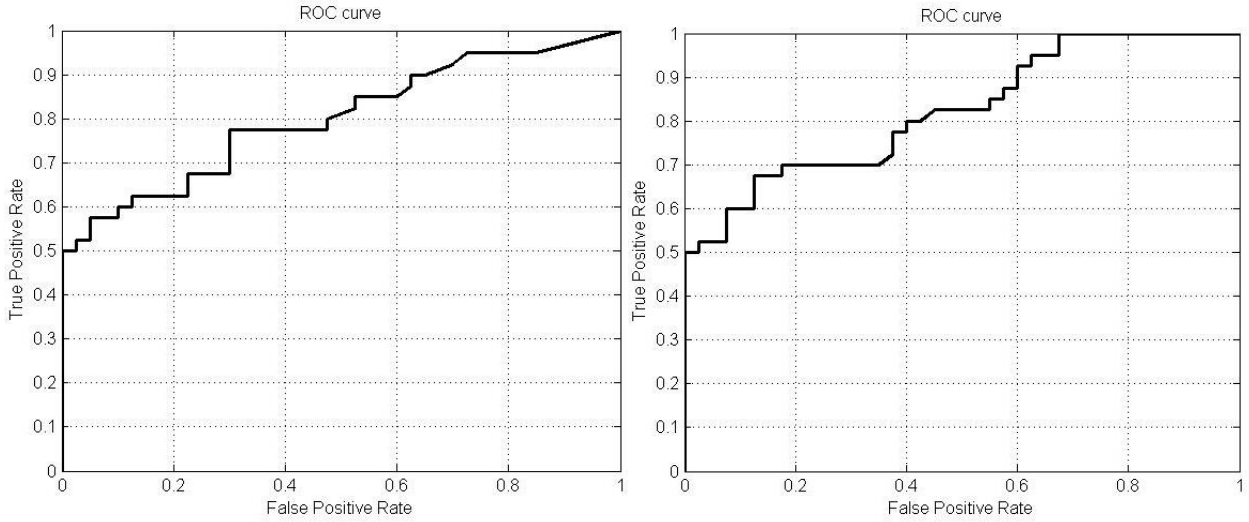

Figure 10 – ROC curves for (a) full shape/surface model and (b) simple model

6. CONCLUSIONS

This paper demonstrates that a simple shape/surface model can be created and used in an estimation filter to estimate parameters about the model. Specifically, in this example the east-west articulation angle offsets of the solar panels from exact sun-tracking is estimated and evaluated as to whether it is 'nominal' or 'anomalous'. It demonstrates that an exquisite and complex shape/surface model is not required in all circumstances when using an estimation filter and opens up the possibility of building a shape/surface model "from scratch" one facet at a time.

7. ACKNOWLEDGEMENTS

This work is sponsored by a Small Business Innovative Research (SBIR) contract FA9451-13-C-0093 through the Air Force Research Laboratory (AFRL).

8. REFERENCES

[1] Calef, B., Africano, J. Birge, B., Hall, D. and Kervin, P., "Photometric Signature Inversion," *Proc. SPIE 6307*, 63070E, 2006.

[2] Wetterer, C. J. & Jah, M. K., "Attitude estimation from light curves," *Journal of Guidance, Control, and Dynamics*, Vol. 32, 2009, pp. 1648-1651.

[3] Julier, S. J., and Uhlmann, J. K., "A New Extension of the Kalman Filter to Nonlinear Systems," *Proceedings of SPIE: The International Society for Optical Engineering*, Vol. 3068, Apr. 1997, pp. 182–193. doi:10.1117/12.280797.

[4] van der Merwe, R., and Wan, E. A., "The Square Root Unscented Kalman Filter for State and Parameter-Estimation," *2001 IEEE International Conference on Acoustics, Speech, and Signal Processing*, Vol. 6, Inst. of Electrical and Electronics Engineers, Piscataway, NJ, May 2001, pp. 3461–3464.

[5] Wetterer, C. J., Crassidis, J. L., Linares, R., Chow, C. C., and Jah, M. K., "Simultaneous Position, Velocity, Attitude, Angular Rates, and Surface Parameter Estimation Using Astrometric and Photometric Observations," *Proceedings of the FUSION Conference*, Istanbul, Turkey, Jul 2013.

[6] Linares, R., Crassidis, J. L., Wetterer, C. J., Hill, K., and Jah, M. K., "Astrometric and Photometric Data Fusion for Mass and Surface Material Estimation using Refined Bidirectional Reflectance Distribution Functions-Solar Radiation Pressure Model," *Advanced Maui Optical and Space Surveillance Technologies (AMOS) conference*, Wailea, Maui, HI, Sep 2013.

[7] Wetterer, C. J., Hunt, B., Hamada, K., Crassidis, J. L., and Kervin, P., "Shape, Surface Parameter, and Attitude Profile Estimation using a Multiple Hypothesis Unscented Kalman Filter," AAS 14-303, *24th AAS/AAIA Spaceflight Mechanics Meeting*, Santa Fe, NM, Jan 2014.

[8] Schmidt, S. F., "Application of state-space methods to navigation problems," *Advances in Control Systems*, vol. 3, 1966, pp. 293–340.

[9] Stauch, J. & Jah, M., "On the Unscented Schmidt Kalman Filter," IEEE paper (unpublished).

[10] Wetterer, C. J., Hunt, B., Kervin, P., and Jah, M. K., "Comparison of Unscented Kalman Filter and Unscented Schmidt Kalman Filter in predicting attitude and associated uncertainty of geosynchronous satellite," The Advanced Maui Optical and Space Surveillance Technologies Conference, Wailea, Maui, Hawaii, 2014 September 9-12 (Maui Economic Development Board).

[11] van der Merwe, R., Doucet, A., de Freitas, J.F.G, and Wan, E., "The Unscented Particle Filter," *Technical Report CUED/F-INFENG/TR 380*, Cambridge University Engineering Department, 2000.

[12] Magill, D. T., "Optimal Adaptive Estimation of Sampled Stochastic Processes," IEEE Transactions on Automatic Control, Vol. AC-10, No. 4, Oct. 1965, pp. 434-439.

[13] Linares, R., Crassidis, J. L., Jah, M. K., & Kim, H., "Astrometric and photometric data fusion for resident space object orbit, attitude, and shape determination via multiple-model adaptive estimation," *AIAA Guidance, Navigation, and Control Conference*, Toronto, Canada, Aug 2010.

[14] Cook, R. L., and Torrance, K. E., "A reflectance model for computer graphics," *ACM Transactions on Graphics*, Vol. 1, No. 1, Jan 1982, pp. 7–24.